










On the plasma permeability of highly porous ceramic framework materials using polymers as marker materials

M. Leander Marxen¹  | Luka Hansen¹  | Armin Reimers²  |
Tim Tjardts³  | Lena M. Saure²  | Erik Greve² | Jonas Drewes³  |
Fabian Schütt²  | Rainer Adelung²  | Holger Kersten¹ 

¹Plasma Technology, Institute of Experimental and Applied Physics, Kiel University (CAU), Kiel, Germany

²Functional Nanomaterials, Faculty of Engineering, Institute of Material Science, Kiel University (CAU), Kiel, Germany

³Multicomponent Materials, Faculty of Engineering, Institute of Material Science, Kiel University (CAU), Kiel, Germany

Correspondence

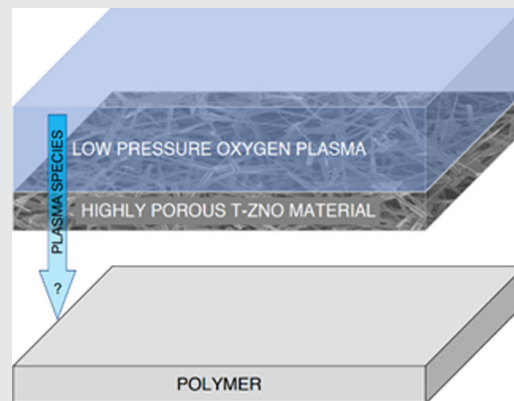
M. Leander Marxen, Plasma Technology, Institute of Experimental and Applied Physics, Kiel University, Kiel 24118, Germany.
Email: marxen@physik.uni-kiel.de

Funding information

Deutsche Forschungsgemeinschaft, Grant/Award Numbers: Project Number 413664940, Grant Number KE 574/8-1

Abstract

Highly porous framework materials are of large interest due to their broad potential for application, for example, as sensors or catalysts. A new approach is presented to investigate, how deep plasma species can penetrate such materials. For this purpose, a polymer (ethylene propylene diene monomere rubber) is used as marker material and covered with the porous material during plasma exposure. Water contact-angle and X-ray photoelectron spectroscopy measurements are used to identify changes in the polymer surface, originating from the interaction of plasma species with the polymer. The method is demonstrated by studying the plasma permeability of tetrapodal zinc oxide framework materials with a porosity of about 90% in an oxygen low-pressure capacitively coupled plasma. Significant differences in the penetration depth ranging from roughly 1.6–4 mm are found for different densities of the material and different treatment conditions.



KEYWORDS

low-pressure discharges, plasma permeability, polymer activation, porous materials, tetrapodal zinc oxide

Abbreviations: CCP, capacitively coupled plasma; EPDM, ethylene propylene diene monomere rubber; HR, high resolution; rf, radio frequency; SEM, scanning electron microscope; t-ZnO, tetrapodal zinc oxide; UHV, ultra high vacuum; WCA, water contact-angle; XPS, X-ray photoelectron spectroscopy.

This is an open access article under the terms of the Creative Commons Attribution License, which permits use, distribution and reproduction in any medium, provided the original work is properly cited.

© 2022 The Authors. *Plasma Processes and Polymers* published by Wiley-VCH GmbH.

1 | INTRODUCTION

The properties of zinc oxide (ZnO) such as for example, being a high band gap semiconductor, chemically stable, and biocompatible resulted in extensive research and a wide range of applications such as gas sensing or catalysis.^[1–5] Tetrapodal zinc oxide (t-ZnO) became a focus of research as individual tetrapod-shaped ZnO crystals can interconnect and form a network of interconnected tetrapods.^[6] This results in a 3D structured, highly porous framework material with a large surface-to-volume ratio.

Controlling the crystal morphology and defect structure of the t-ZnO enables adaptation to the different applications. Plasma treatment of ZnO showed promising results in modifying ZnO by, for example, plasma etching^[7–15], to improve its properties^[16–18], such as p-type conductivity^[17]. To combine the advantages of the 3D highly porous t-ZnO with modifications gained by plasma treatment, plasma penetration into the 3D structure is necessary.

Further, the plasma itself can be strongly affected by plasma-surface-interactions like secondary electron emission.^[19–24] Thus, usage of the large surface-to-volume ratio of t-ZnO as electrode material could enhance plasma properties, especially, for microplasmas, where the surface-to-volume ratio is already quite large.^[25–27]

Other examples, like plasma catalysis^[28–31], also showcase applications where the penetration of plasma species into the highly porous t-ZnO material is favorable if not necessary. Thus, in this study, we present a simple and convenient approach to determine the plasma

permeability of highly porous materials using the example of t-ZnO framework materials.

In the past, investigations were made to study, for example, the transmission of N-atoms in the afterglow of a microwave discharge through porous materials like sterilization pouches (2D structured materials).^[32,33] Canal et al. used hydrophobic textiles as indicator material behind the porous sheet. For those textiles, the wetting time was measured after plasma exposure.^[33] The t-ZnO framework materials, which were studied in this work, feature a truly 3-dimensional porous structure.^[6] The hydrophobic textile was replaced with a suitable polymer as marker material, which offers an even easier method to determine the plasma permeability of porous materials. Figure 1 shows the idea schematically.

The interaction of plasma with polymer surfaces has been described in many publications and textbooks.^[34–40] Oversimplified summarizing, high energy plasma particles and UV-radiation lead to dissociations of the C–C and C–H-bonds. Thus, other atoms or groups can be attached to the C-radical sites, depending on the reactive species in the plasma. Exposing a polymer to an oxygen plasma leads to functionalization of the polymer surface by the attachment of oxygen-containing polar groups, as sketched with OH-groups as an example in Figure 1. One expects to detect C–O–C, C–O–H, C–O–O–H, and C=O bonds within the C 1s-peak of an XPS high-resolution (HR) scan of the surface.

This functionalization leads to a decreased water contact angle (WCA) and a higher oxygen ratio on the surface of the polymer. Depending on the chosen

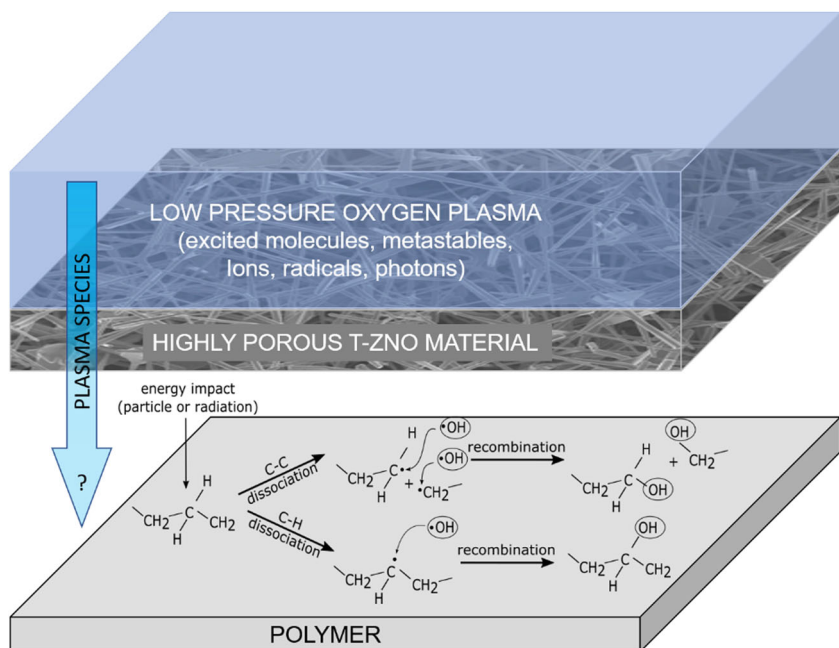


FIGURE 1 Schematic illustration of the indirect approach. If plasma species permeate the highly porous tetrapodal zinc oxide (t-ZnO) framework material, they will modify the surface of the polymer marker material. In the real setup, the gap between the t-ZnO and the polymer does not exist (see Figure 2b).

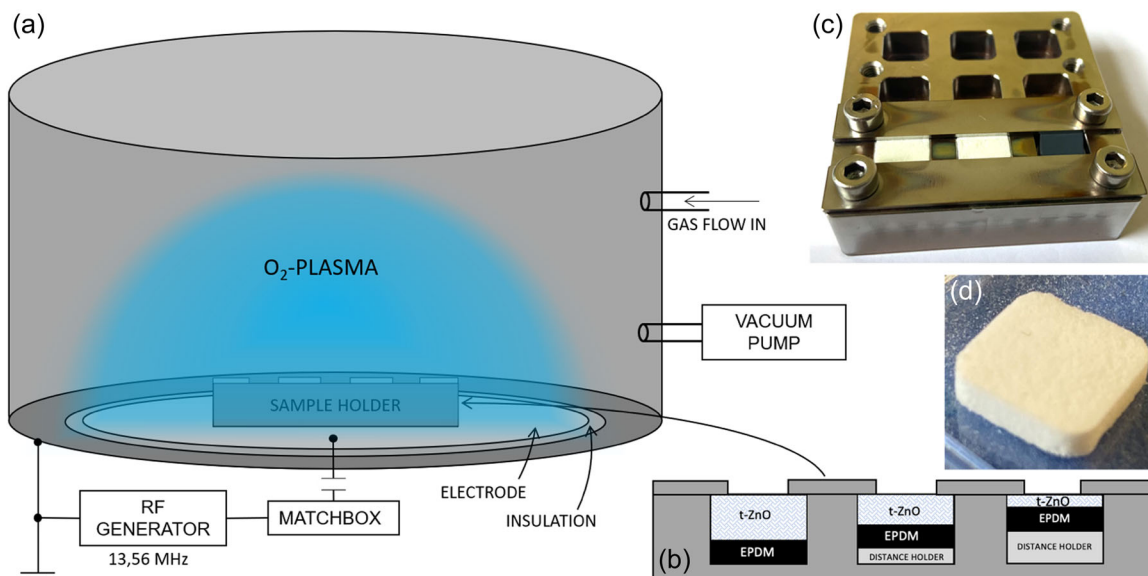


FIGURE 2 (a) Setup for the plasma chamber. (b) Schematic of the sample holder for ethylene propylene diene monomere rubber (EPDM) test polymer covered by tetrapodal zinc oxide (t-ZnO). There is no possibility for the plasma species to reach the EPDM surface directly without permeating the t-ZnO sample. (c) Photograph of the filled stainless-steel sample holder with t-ZnO covers on two samples (left and middle) and pristine EPDM on the right. (d) Photograph of a 2.5 mm thick t-ZnO sample.

polymer and plasma parameters, significant differences in surface modification can easily be measured. Thus, a suitable polymer can be used as an indicator material to study, if plasma can permeate through highly porous 3D structures, which are placed on top of it.

2 | EXPERIMENTAL SECTION

The experiments were performed in an oxygen (Air Liquide, 99.9999% purity) low-pressure CCP.^[41–43] This comes with the advantage of low mechanical impact on the studied material samples compared to strong gas flows using atmospheric pressure plasma jets.^[44] The walls of the plasma chamber are used as the grounded electrode, which results in a large geometric asymmetry (Figure 2a). Hence, a negative self-bias occurs, which has been described elsewhere.^[41,45]

The change of the WCA of the EPDM surface due to oxygen plasma treatment was found to be high in comparison to other for us available polymers (e.g., polyethylene or polypropylene) in former, unpublished measurements of our group. Hence, it was chosen as suitable marker material. Untreated EPDM has a WCA of about 130°. A parameter study was performed to determine the pressure p , rf-plasma power P_{RF} , and treatment time t , for which the maximum change in WCA is observed. The smallest WCA (30°) was found for $p = 10$ Pa, $P_{RF} = 80$ W and $t = 6$ min. The selfbias is

roughly -700 V. These conditions were realized for all further experiments.

To guarantee the same plasma conditions for t-ZnO samples of varying thicknesses, a sample holder was constructed, which is schematically shown in Figure 2b. A photograph of the holder when typically filled for the experiment is shown in Figure 2c. The whole setup with the sample holder in the plasma chamber is sketched in Figure 2a.

To gain insight into the penetrating species (ions or neutral components like atomic oxygen, molecular oxygen or ozone), different holder potentials were realized. One holder was made out of stainless steel, one was made out of Teflon. The positioning inside the chamber was varied between in the plasma sheath (directly on the rf-electrode, Figure 3a,b) and in the plasma bulk. To lift the holder into the bulk, glass cylinders (height about 4 cm, Figure 3c) were used. In the bulk, the holder acts as a floating body with a floating potential of approximately -10 V. On the rf-electrode, the stainless-steel holder will adopt the negative self-bias potential. In contrast, the Teflon holder will be like a dielectric barrier in front of the electrode. The changes in the sheath configuration are even visible the naked eye (Figure 3).

It was also investigated, if any change in the behavior of the t-ZnO samples is obtained, when they are exposed to the plasma multiple times. For this, the stainless-steel holder was placed in the sheath and in the bulk.

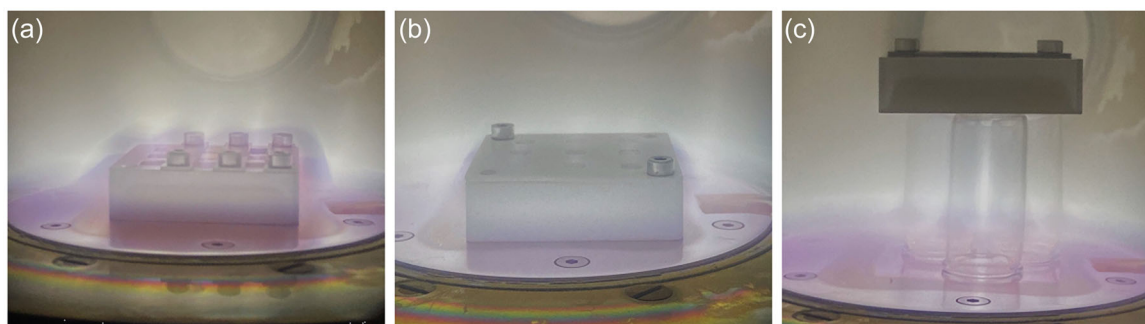


FIGURE 3 Different materials of the sample holders and different positions in the plasma chamber lead to different sheath configurations in front of the tetrapodal zinc oxide (t-ZnO)/ethylene propylene diene monomere rubber (EPDM) substrate. (a) Stainless steel holder on the rf-electrode/in the sheath. (b) Teflon holder on the rf-electrode/in the sheath. (c) Stainless steel holder on glass cylinders and, thus, lifted into the plasma bulk. There is no visible sheath for this configuration.

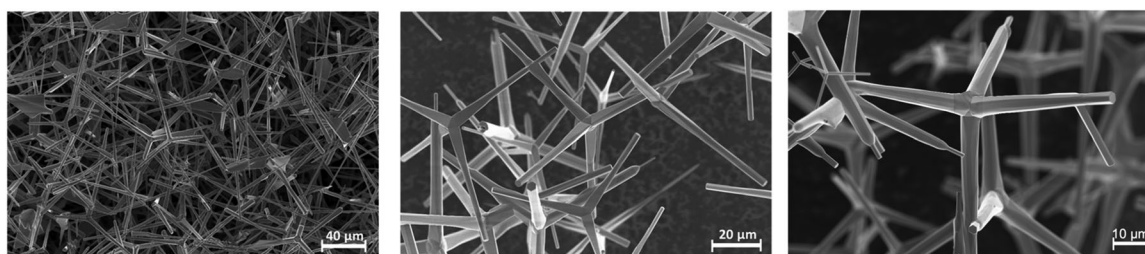


FIGURE 4 Scanning electron microscope pictures of the investigated tetrapodal zinc oxide (t-ZnO) samples with a mass density of 0.3 g cm^{-3} at different scales

WCA measurements were used as a fast and easy method to determine changes in the surface tension due to plasma species that have permeated the t-ZnO material.^[46–48] The sessile-drop method^[46] was conducted via a custom-built setup. More precise information was obtained by XPS.^[46] It was performed for samples in both holders for placement in the sheath. The goal was to prove that the reduced WCA arises from oxygen-containing polar groups, which were formed on the EPDM surface underneath the covering highly porous 3D structures during the plasma exposure. The XPS measurements were conducted with an XPS UHV system (PREVAC Sp. z o. o.) at a pressure of 10^{-9} mbar. An Aluminum anode X-ray tube operated at 300 W (15 kV, 20 mA) was utilized as an X-ray source. Survey scans were conducted at three iterations and a pass energy of 200 eV, while HR scans were performed at 20 iterations and a pass energy of 50 eV. The charge correction was done with the C 1s main peak at 284.8 eV.

The production of the t-ZnO (Flame Transport Synthesis) was described by Gedamu et al. elsewhere.^[49] It was pressed into 10×10 mm samples of varying thickness, which were then sintered for 5 h at 1150°C (Figure 2d contains a 2.5 mm thick sample as an

example). Figure 4 shows pictures of a 0.3 g cm^{-3} density t-ZnO framework in different scales, obtained by scanning electron microscopy (SEM). The randomly distributed arms of the ZnO tetrapods form an interconnected network, creating a completely open porous framework material. The porosity of this framework material in % can be calculated by comparing the network's density with the bulk density of ZnO ($\rho_{\text{ZnO}} = 5.61 \text{ g cm}^{-3}$) using the formula $\phi = \left(1 - \frac{\rho_{\text{network}}}{\rho_{\text{ZnO}}}\right) * 100$.^[44]

Most of the investigated t-ZnO framework material samples have mass densities of 0.3 g cm^{-3} , which corresponds to a porosity of $\phi = 94.7\%$. For the stainless-steel holder in the sheath, t-ZnO samples of thicknesses between 1.0 and 2.5 mm were investigated. For the Teflon holder in the sheath, the t-ZnO samples had thicknesses from 1.0 to 5.0 mm. Measurements for multiple usages of the same t-ZnO samples in the sheath and in the bulk were made for t-ZnO with a thickness of 1.6 mm. For 1.3 mm thick t-ZnO samples, densities of 0.45 g cm^{-3} ($\phi = 92.0\%$) and 0.6 g cm^{-3} ($\phi = 89.3\%$) were studied. They were placed in the sheath using the stainless-steel holder.

3 | RESULTS AND DISCUSSION

For placing the stainless-steel holder directly on the rf-electrode, the thickness of the covering material is varied between 1.0 and 2.5 mm. The samples have a mass density of 0.3 g cm^{-3} . In Figure 5, the results for the EPDM examination after the plasma exposure are shown. All depicted results for the performed WCA measurements include error bars originating from repetitions of the experiments. The WCA and XPS values for uncovered (dark green in Figure 5, WCA of $[24 \pm 6]^\circ$) and untreated (red, WCA of $[136 \pm 5]^\circ$) EPDM markers can be considered as references. Figure 5a illustrates the increasing WCA if thicker t-ZnO samples cover the EPDM during the plasma exposure. Starting at $(24 \pm 6)^\circ$ for the uncovered EPDM, the WCA increases to $(56 \pm 16)^\circ$ for 1.0 mm, to $(70 \pm 19)^\circ$ for 1.3 mm, and to

$(84 \pm 25)^\circ$ for 1.6 mm, until it reaches values between 130° and 140° for covering thicknesses of 1.9 mm and thicker. A WCA in this region means no significant change in the surface tension of the marker polymer. These results are very intuitive, as they reveal a better permeability for thinner covers. There are large error bars when a treatment effect underneath the cover occurs (1.0–1.6 mm). The reason for this is probably that the treatment effect on the covered EPDM changes dramatically for little inhomogeneities of the porous material samples. Nevertheless, there is a nonneglectable increasing trend of the WCA in the data for thicker covers.

It is yet to validate that this effect truly is due to oxygen-containing functional groups generated at the EPDM surface and, thus, it is a plasma treatment effect. The XPS measurement (Figure 5b) delivers this

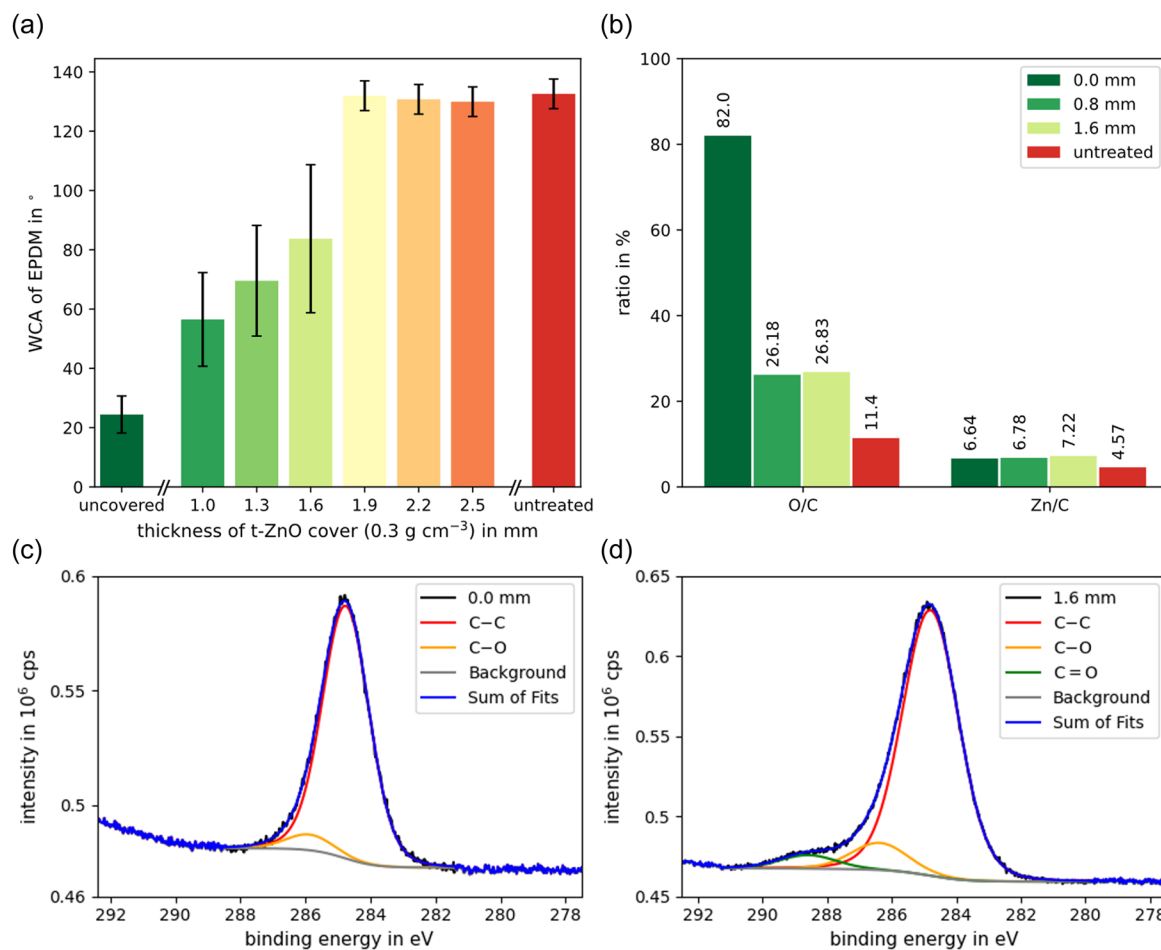


FIGURE 5 Results for different thicknesses of tetrapodal zinc oxide (t-ZnO) covers. The mass density of the t-ZnO is 0.3 g cm^{-3} , the stainless-steel holder was used and placed directly on the rf-electrode. (a) Water contact-angle (WCA) and (b) X-ray photoelectron spectroscopy (XPS) data for the ethylene propylene diene monomere rubber (EPDM) surface after the plasma exposure. (a, b) Include data for untreated EPDM (red bars) and uncovered EPDM (dark green bars), which can be regarded as reference values. (c) High resolution (HR) scan of the C 1s-peak for uncovered EPDM after the plasma exposure. (d) HR scan of the C 1s-peak for EPDM, which was covered with 1.6 mm t-ZnO during the plasma exposure.

information. Data were acquired for pristine EPDM before (untreated) and after plasma exposure (uncovered) as well as for EPDM that was covered with t-ZnO samples. The samples had thicknesses of 0.8 mm and 1.6 mm and a mass density of 0.3 g cm^{-3} . The results show an extreme increase in the O/C ratio for the uncovered EPDM from 11.4%–82.0%. For the covered EPDM, there is still a significant increase in the O/C ratio. A value of more than 26% was observed for both t-ZnO thicknesses. The Zn/C ratio is in the same range (4.5%–7%) for all EPDM samples. This reveals only a small ZnO contamination of the EPDM surface. HR XPS scans of the C 1s-peak (Figure 5c,d) show that C–O ($\sim 286 \text{ eV}$ ^[40]) and C=O ($\sim 289 \text{ eV}$ ^[40]) bonds were formed at the EPDM surface. Hence, the large increase in the O/C ratio will originate from oxygen-containing functional groups (and not from ZnO contamination). These results allow concluding that plasma species can permeate through the highly porous t-ZnO networks.

Summarizing the above, the larger wettability of the EPDM surface, measured by WCA, can be attributed to functionalization of the polymer and does not originate from ZnO leftovers on the surface. Furthermore, the penetration depth of plasma species into the t-ZnO framework material of 0.3 g cm^{-3} can be estimated as approximately 1.6 mm under these conditions.

Considering that plasma species (in particular: oxygen radicals/ions) can permeate the porous framework material, parameters and experimental conditions were varied. The t-ZnO density, the material of the sample holder, and the position in the plasma chamber are changed to investigate their influence on the permeability.

A higher mass density of the t-ZnO cover should lead to a weaker plasma treatment effect on the EPDM surface. Figure 6 confirms at least the trend for this expectation. Taking the large error for frameworks of 0.3 g cm^{-3} density into account ($70 \pm 19^\circ$), it can be concluded that the assumption should be right. The highest studied mass density of a t-ZnO sample is 0.6 g cm^{-3} , which hardly leads to any effect on the EPDM surface ($127 \pm 6^\circ$).

Figure 7 shows that the holder material plays a major role in the permeation through the t-ZnO samples. The Teflon holder was used in the sheath to gain insight into the influence of the holder's potential. The different sheath configurations for the two holders are visible by the naked eye (Figure 3a,b). The WCA for a thickness variation of the t-ZnO samples is depicted in Figure 7a. The blue bars show the values for the Teflon holder. A much better treatment effect on the EPDM surface for all thicknesses (including uncovered EPDM treatment) relative to the stainless-steel holder is observed. For the

t-ZnO in the stainless-steel holder, there is no change in the WCA compared to the untreated EPDM for covering thicknesses larger than 1.9 mm. In contrast, there is just a relatively small change between uncovered treated EPDM ($8 \pm 5^\circ$) and a cover thickness of 1.9 mm ($24 \pm 5^\circ$) in the Teflon holder. Even for a thickness of 4 mm, there is still a small effect in the contact angle of the EPDM ($126 \pm 7^\circ$) if using the Teflon holder.

The XPS measurements in Figure 7b confirm the WCA results. The O/C ratio of the EPDM, which was covered with 1.6 mm thick t-ZnO in the Teflon holder, is 32.55%. This is about 6% higher than in the stainless steel holder. Another important result of the XPS measurement is the fluorine ratio F/C. Since Teflon is not inert to plasma^[50], fluorine compounds could also be responsible for the smaller WCA values. However, there is no significant F/C ratio for the EPDM that was covered with the t-ZnO. Figure 7c shows an HR XPS scan for binding energies, at which fluorine would be detected.^[51,52] A clear peak is found only for the uncovered EPDM sample in the Teflon holder. In Figure 7d, C–O and C=O bonds can be found as subpeaks in the C 1s-peak of the EPDM, which was covered with 1.6 mm t-ZnO during the plasma exposure. C–F bonds would have been detected at binding energy between 293 and 294 eV.^[51] They are not found in these measurements. Hence, the smaller WCA originates from the higher oxygen ratio and not from fluorine compounds. Additional EDX (energy dispersive X-ray spectroscopy)^[53] measurements also showed no significant fluorine concentration in the t-ZnO samples, which were used in the Teflon holder. Thus, released fluorine will not be responsible for the enhanced plasma permeability in the Teflon holder.

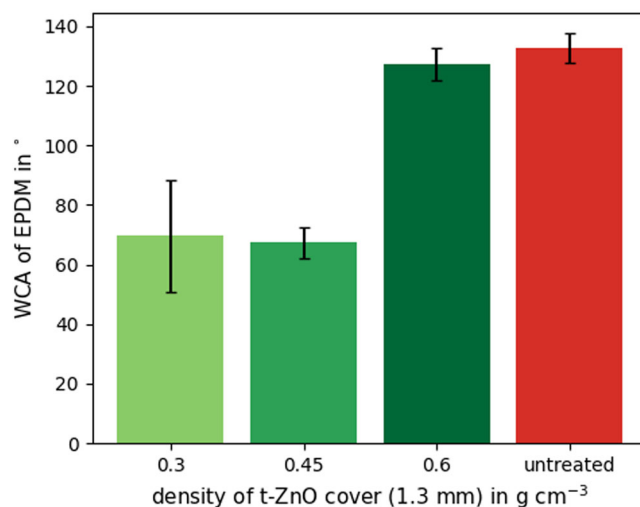


FIGURE 6 Variation of the mass density of the tetrapodal zinc oxide (t-ZnO) samples. The samples were used in the stainless-steel holder in the sheath

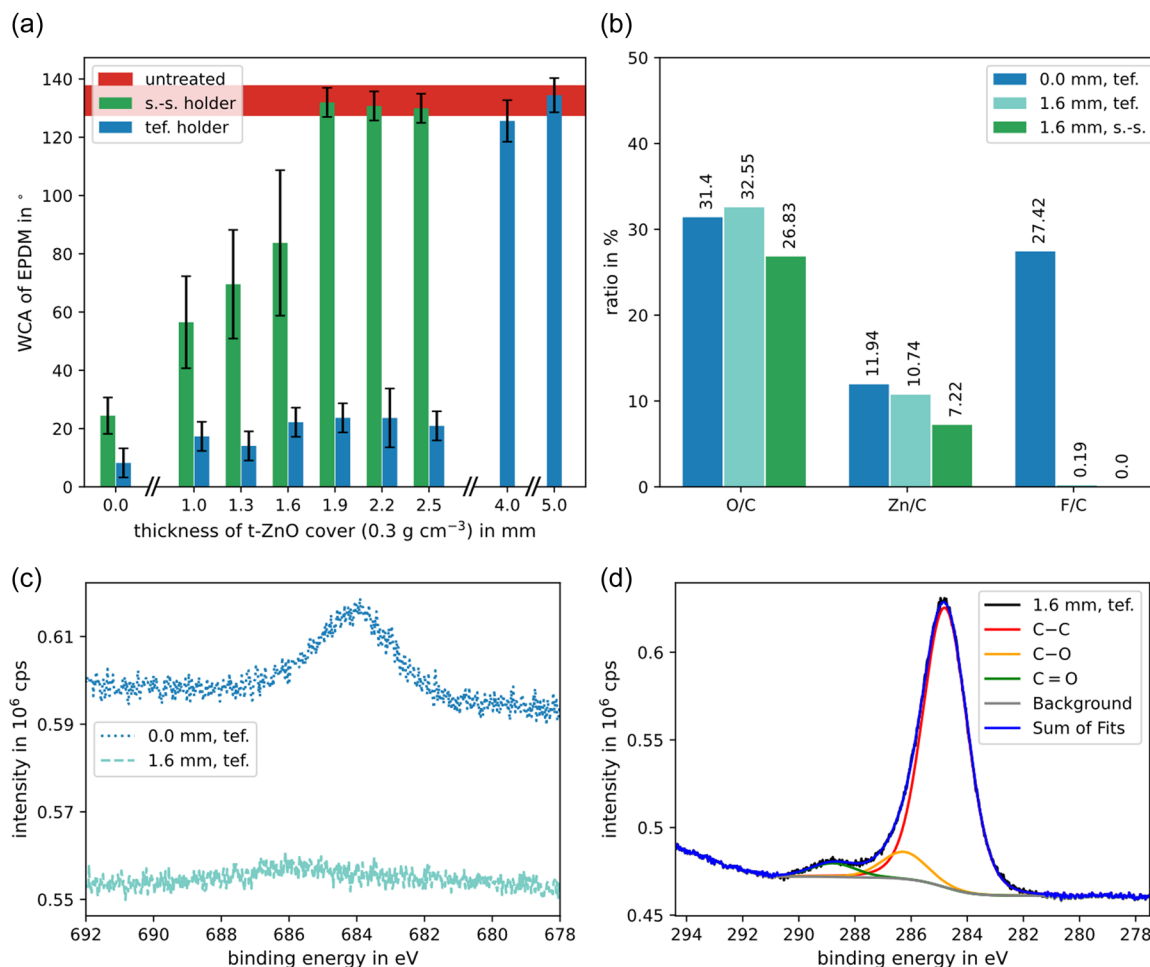


FIGURE 7 Comparison of the Teflon (tef.) holder (blue bars) and the stainless-steel (s.-s.) holder (green bars). Both holders were placed in the sheath. (a) Water contact-angle results. For values $\leq 15^\circ$, the water drop was covering almost the complete ethylene propylene diene monomere rubber (EPDM) surface. (b) X-ray photoelectron spectroscopy (XPS) examined surface composition. (c) High resolution (HR) scan of the F 1s-peak. (d) HR scan of the C 1s-peak for EPDM which was covered with 1.6 mm t-ZnO during the plasma exposure in the Teflon holder.

A possible explanation for better surface activation in the Teflon holder compared to the stainless-steel holder could be the following. The stainless-steel holder on the rf-electrode adopts the self-bias potential of roughly -700 V. The t-ZnO samples, instead, will not adopt this potential and will be less negatively charged. Thus, positive ions are deflected in their trajectories and attracted toward the stainless-steel of the holder. This could work similar as a defocusing ion lens. It would result in fewer ions arriving at the top t-ZnO and permeating it towards the bottom EPDM. The Teflon holder instead works like a dielectric barrier in front of the electrode and will not influence the trajectories of the arriving species as much.

To investigate changes in the plasma permeability of the t-ZnO for multiple plasma exposures, four samples of 1.6 mm thickness were used three times each. An unused EPDM sample was placed underneath the t-ZnO for

every run. Figure 8a shows the WCA results. It holds values for positioning in the sheath (light green) and in the bulk (darker green). The different positions result in different sheath configurations (Figure 3). The uncovered EPDM has a WCA of $(79 \pm 5)^\circ$ after being treated in the bulk. In the bulk, the ions, which arrive at the samples, have smaller kinetic energy compared to sample placement in the sheath. This explains, why the overall WCA values are higher for treatment in the bulk. The covered EPDM showed a WCA of about 120° for all three usages of the t-ZnO in the bulk. In contrast, for treatment in the sheath, the WCA decreases with every usage of the t-ZnO samples. (Note: The value for the first use in the sheath differs from the value for 1.6 mm in Figure 5a. That is, because only those samples were considered here, which were truly used multiple times). For the first use, the WCA of the EPDM underneath is $(76 \pm 8)^\circ$, for the second use $(57 \pm 12)^\circ$ and for the third use $(44 \pm 9)^\circ$.

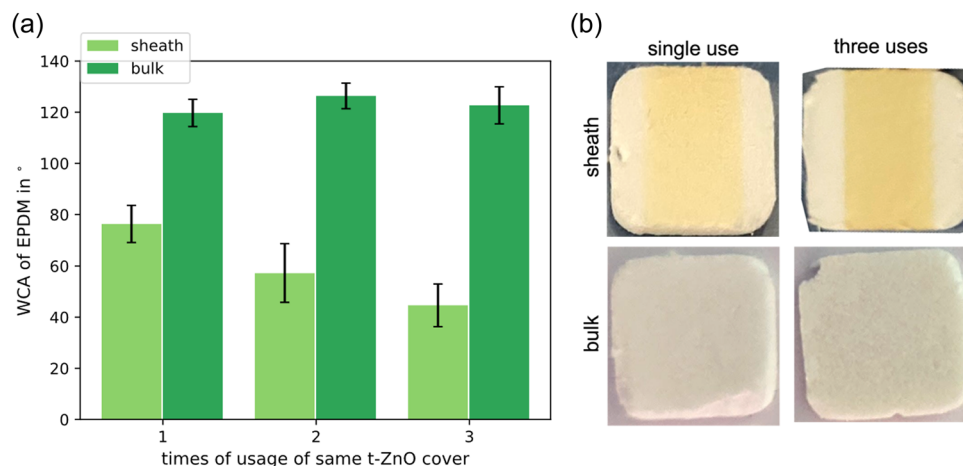


FIGURE 8 Multiple usage of the same tetrapodal zinc oxide (t-ZnO) samples. The samples had a thickness of 1.6 mm and a mass density of 0.3 g cm^{-3} . The stainless steel holder was used. (a) Water contact-angle results. A comparison is made for plasma exposure in the sheath/directly on the rf-electrode (light green) versus in the bulk (darker green). (b) Photos of the t-ZnO samples after the plasma exposure.

Thus, plasma exposure of the t-ZnO in the sheath enhances its plasma permeability.

This also hints toward the species that play a major role in the functionalization of the polymer surface underneath the t-ZnO. In the bulk, the ions are not accelerated to the samples as much as in the sheath (the potential of the holder is roughly -10 to -20 V in comparison to -700 V). On the other hand, neutral species like atomic and molecular oxygen or ozone are barely affected by the different electrical configurations in the bulk. They will even be present at higher densities. Thus, one can assume that ions from the discharge are the major species permeating the porous t-ZnO material. Further, the role of UV-photons will be negligible for the same reason and EPDM was found to be resistant to UV radiation within the short treatment times used in this study.^[54]

In Figure 8b, photos of the t-ZnO samples are shown. The samples in the upper row were exposed to the plasma in the sheath, in the lower row in the bulk. The left photos were taken after the first use and the right photos after the third use of the samples. For positioning in the sheath, an increasing yellowish color change is visible. In contrast, the samples in the bulk do not change in color. A yellowish color change indicates an increase in excess zinc ions in the t-ZnO crystal structure.^[55] The enrichment in zinc ions can occur due to oxygen radicals and ions in the plasma, which are binding oxygen atoms from the zinc oxide. The resulting change in conductivity of the t-ZnO could also influence the permeability of the material. Proving this hypothesis could be a subject of future experiments.

One could also imagine a sputtering effect for the position in the sheath, which would lead to an increase

in porosity. This would enhance the plasma permeability as well. However, SEM of the used samples did not reveal any mechanical changes to the network structure.

4 | CONCLUSION

Summarizing the performed experiments, this study can be regarded as a proof of principle for the method of using polymers as marker materials to study the plasma permeability of highly porous framework materials. The results by WCA and XPS measurements emphasize that porous framework materials produced from t-ZnO possess a plasma permeability in an oxygen low-pressure CCP. The permeability decreases with increasing sample thickness and mass density of the t-ZnO framework. XPS examination validates that oxygen ions and/or radicals modify the covered polymer. The O/C ratio increases from roughly 11% for untreated EPDM to more than 26% for EPDM, which was covered with 1.6 mm thick t-ZnO during the plasma exposure. C–O and C=O bonds on the EPDM surface were detected in HR XPS scans. It was found that the treatment conditions, such as positioning in the plasma chamber and material of the sample holder, play a significant role. The penetration depth was found to be approximately 1.6 mm for t-ZnO (mass density 0.3 g cm^{-3}) when placed in a stainless steel holder directly on the rf-electrode. Using a Teflon holder instead, showed a much larger penetration depth between 2.5 and 4 mm. Exposing t-ZnO samples to the plasma directly on the rf-electrode multiple times enhances the permeability. This was observed by a decreasing WCA from $(76 \pm 8)^\circ$ (first use) to $(44 \pm 9)^\circ$ (third use). This effect was not

obtained for positioning in the plasma bulk. The smaller effects on the covered EPDM in the bulk in general hint toward the ions as being the dominant species for the permeation of the porous network structures. Further understanding of the plasma permeability could be gathered, for example, by covering a mass spectrometer instead an EPDM marker with the porous framework materials to quantify the permeating species.

AUTHOR CONTRIBUTIONS

M. Leander Marxen was involved in conceptualization, performing the experiments, examining the results, and writing – the original draft. Luka Hansen was involved in conceptualization, examining the results, and writing – the original draft. Armin Reimers, Lena M. Saure, and Erik Greve were involved in producing the t-ZnO samples and writing – reviewing, and editing. Tim Tjardts and Jonas Drewes were involved in performing and examining the XPS results and writing – reviewing and editing. Fabian Schütt was involved in writing – reviewing and editing. Rainer Adelung was involved in conceptualization. Holger Kersten was involved in conceptualization, examining the results, and writing – reviewing, and editing.

ACKNOWLEDGMENTS

We would like to thank Margarethe Hauck for helping with the production of t-ZnO samples. Further, we would like to thank Frank Bach and Volker Rohwer for their technical assistance. Funding from the German Research Foundation (DFG, Project Number 413664940, Grant Number KE 574/8-1) is gratefully acknowledged. Open access funding enabled and organized by Projekt DEAL.

CONFLICT OF INTEREST

The authors declare no conflict of interest.

DATA AVAILABILITY STATEMENT

The data that support the findings of this study are available from the corresponding author upon reasonable request.

ORCID

M. Leander Marxen  <http://orcid.org/0000-0002-6457-5888>

Luka Hansen  <http://orcid.org/0000-0003-2656-4069>

Armin Reimers  <http://orcid.org/0000-0001-5225-6815>

Tim Tjardts  <http://orcid.org/0000-0002-0474-3165>

Lena M. Saure  <http://orcid.org/0000-0001-7714-5222>

Jonas Drewes  <http://orcid.org/0000-0002-8539-1543>

Fabian Schütt  <http://orcid.org/0000-0003-2942-503X>

Rainer Adelung  <http://orcid.org/0000-0002-2617-678X>

Holger Kersten  <http://orcid.org/0000-0003-1798-7588>

REFERENCES

- [1] C. Klingshirn, *ChemPhysChem* **2007**, *8*, 782.
- [2] A. Kolodziejczak-Radzimska, T. Jesionowski, *Materials* **2014**, *7*, 2833.
- [3] J. Theerthagiri, S. Salla, R. A. Senthil, P. Nithyadharseni, A. Madankumar, P. Arunachalam, T. Maiyalagan, H.-S. Kim, *Nanotechnology* **2019**, *30*, 392001.
- [4] Ü. Özgür, D. Hofstetter, H. Morkoc, *IEEE* **2010**, *98*, 1255.
- [5] K. V. Gurav, M. G. Gang, S. W. Shin, U. M. Patil, P. R. Deshmukh, G. L. Agawane, M. P. Suryawanshi, S. M. Pawar, P. S. Patil, C. D. Lokhande, J. H. Kim, *Sensor Actuat. B Chem.* **2014**, *190*, 439.
- [6] Y. Mishra, R. Adelung, *Mater. Today* **2018**, *21*, 631.
- [7] D. Gruber, F. Kraus, J. Müller, *Sensor Actuat. B Chem.* **2003**, *92*, 81.
- [8] S.-J. Chen, C.-M. Chang, J.-S. Kao, F.-R. Chen, C.-H. Tsai, *Sci. Technol. A* **2010**, *28*, 745.
- [9] K. K. Lee, Y. Luo, X. Lu, P. Bao, A. M. Song, *IEEE Nanotechnol.* **2011**, *10*, 839.
- [10] L. Wang, X. Zhang, Y. Zhao, T. Yamada, Y. Naito, *Appl. Surf. Sci.* **2014**, *316*, 508.
- [11] G. Das, S. Bose, J. R. Sharma, S. Mukhopadhyay, A. K. Barua, J. Mater, *Sci. Mater. Elect.* **2018**, *29*, 6206.
- [12] J.-C. Woo, T.-K. Ha, C. Li, S.-H. Kim, J.-S. Park, K.-M. Heo, C.-I. Kim, *Trans. Elect. Electron. Mater.* **2011**, *12*, 60.
- [13] S. R. Min, H. N. Cho, Y. L. Li, C. W. Chung, *Thin Solid Films* **2008**, *516*, 3521.
- [14] G.-K. Lee, J.-H. Moon, B.-T. Lee, *Semiconduct. Sci. Technol.* **2006**, *21*, 971.
- [15] N. Kohlmann, L. Hansen, C. Lupan, U. Schürmann, A. Reimers, F. Schütt, R. Adelung, H. Kersten, L. Kienle, *ACS Appl. Mater. Inter.* **2021**, *13*, 61758.
- [16] Q. Liu, M. Gong, B. Cook, P. Thapa, D. Ewing, M. Casper, A. Stramel, J. Wu, *Phys. Status Solid.* **2017**, *214*, 1700176.
- [17] P. Cao, D. X. Zhao, J. Y. Zhang, D. Z. Shen, Y. M. Lu, B. Yao, B. H. Li, Y. Bai, X. W. Fan, *Appl. Surf. Sci.* **2008**, *254*, 2900.
- [18] F. Yang, J. Guo, L. Zhao, W. Shang, Y. Gao, S. Zhang, G. Gu, B. Zhang, P. Cui, G. Cheng, Z. Du, *Nano Energy* **2020**, *67*, 104210.
- [19] A. V. Phelps, Z. L. Petrovic, *Plasma Sources Sci.* **1999**, *8*, R21.
- [20] A. V. Phelps, L. C. Pitchford, C. Pedoussat, Z. Donko, *Plasma Sources Sci.* **1999**, *8*, B1.
- [21] M. Daksha, A. Derzsi, Z. Mujahid, D. Schulenberg, B. Berger, Z. Donko, J. Schulze, *Plasma Sources Sci.* **2019**, *28*, 034002.
- [22] R. Hippler, H. Kersten, M. Schmidt, K. Schoenbach, *Low Temperature Plasmas: Fundamentals, Technologies and Techniques*, Wiley-VCH, **2008**.
- [23] M. A. Lieberman, A. J. Lichtenberg, *Principles of Plasma Discharges and Materials Processing*, John Wiley and Sons, **2005**.
- [24] Y. P. Raizer, *Gas Discharge Physics*, Springer Berlin Heidelberg, **2011**.
- [25] K. H. Becker, K. H. Schoenbach, J. G. Eden, *J. Phys. D. Appl. Phys.* **2006**, *39*, R55.
- [26] F. Iza, G. J. Kim, S. M. Lee, J. K. Lee, L. Walsh, Y. T. Zhang, M. G. Kong, *Plasma. Process. Polym.* **2008**, *5*, 322.
- [27] L. Hansen, N. Kohlmann, U. Schürmann, L. Kienle, H. Kersten, *Plasma Sources Sci.* **2022**, *31*, 035013.

- [28] A. Bogaerts, X. Tu, J. C. Whitehead, *J. Phys. D. Appl. Phys.* **2020**, *53*, 3001.
- [29] E. C. Neyts, A. Bogaerts, *J. Phys. D. Appl. Phys.* **2014**, *47*, 224010.
- [30] E. C. Neyts, K. Ostrikov, K. S. Mehandra, A. Bogaerts, *Chem. Rev.* **2015**, *115*, 13408.
- [31] X. Feng, H. Liu, C. He, Z. Shen, T. Wang, *Catal. Sci. Technol.* **2018**, *8*, 936.
- [32] A. Ricard, C. Canal, S. Villegier, J. Durand, *Plasma. Process. Polym.* **2008**, *5*, 867.
- [33] C. Canal, S. Villegier, A. Ricard, *Plasma. Process. Polym.* **2011**, *8*, 505.
- [34] C. M. Chan, T. M. Ko, H. Hiraoka, *Surf. Sci. Rep.* **1996**, *24*, 1.
- [35] A. Vesel, M. Mozetic, *J. Phys. D. Appl. Phys.* **2017**, *50*, 293001.
- [36] J. M. Grace, L. J. Gerenser, *J. Disper. Sci. Technol.* **2003**, *24*, 305.
- [37] L. J. Gerenser, *J. Adhes. Sci. Technol.* **1987**, *1*, 303.
- [38] A. Vesel, M. Mozetic, *Vacuum* **2012**, *86*, 634.
- [39] J. F. Friedrich, R. Mix, R. D. Schulze, A. Meyer-Plath, R. Joshi, S. Wettmarshausen, *Plasma. Process. Polym.* **2008**, *5*, 407.
- [40] J. Friedrich, *The Plasma Chemistry of Polymer Surfaces*, WILEY-VCH, **2012**.
- [41] A. M. Hinz, E. von Wahl, F. Faupel, T. Strunskus, H. Kersten, *J. Phys. D. Appl. Phys.* **2015**, *48*, 055203.
- [42] Y. A. Ussenov, E. von Wahl, Z. Marvi, T. S. Ramazanov, H. Kersten, *Vacuum* **2019**, *166*, 15.
- [43] T. Wegner, A. M. Hinz, F. Faupel, T. Strunskus, H. Kersten, J. Meichsner, *Appl. Phys. Lett.* **2016**, *108*, 063108.
- [44] S. Daria, S. Sindu, M. Hoppe, L. Hansen, J. Marx, J. Dittman, Z. Kareh, B. Fiedler, H. Kersten, R. Adelung, *Contrib. Plasma Phys.* **2018**, *58*, 384.
- [45] M. A. Lieberman, *J. Appl. Phys.* **1989**, *65*, 4186.
- [46] M. Stamm, *Polymer Surfaces and Interfaces. Characterization, Modification and Applications*, Springer, **2008**.
- [47] A. W. Adamson, *Physical Chemistry of Surfaces*, 5th edition., Wiley Interscience, **1990**.
- [48] C. J. van Oss, R. J. Good, M. Chaudhury, *Langmuir* **1988**, *4*, 884.
- [49] D. Gedamu, I. Paulowicz, S. Kaps, O. Lupan, S. Wille, G. Haidarschin, Y. K. Mishra, R. Adelung, *Adv. Mater.* **2013**, *26*, 1541.
- [50] M. K. Shi, L. Martinu, E. Sacher, A. Selmani, M. R. Wertheimer, A. Yelon, *Surf. Interface Anal.* **1995**, *23*, 99.
- [51] C. Girardeaux, J.-J. Pireaux, *Surf. Sci. Spectra* **1996**, *4*, 138.
- [52] S. W. Gaarenstroom, N. Winograd, *J. Chem. Phys.* **1977**, *67*, 3500.
- [53] D. Shindo, T. Oikawa, *Analytical Electron Microscopy for Material Science*, Springer, **2002**, pp. 81.
- [54] B.-H. Youn, C.-S. Huh, *IEEE Dielect. El.* **2005**, *12*, 1015.
- [55] F. van Craeynest, W. Maenhout-van der Vorst, W. Dekeyser, *Phys. Status Solid. B* **1965**, *8*, 841.

How to cite this article: M. L. Marxen, L. Hansen, A. Reimers, T. Tjardts, L. M. Saure, E. Greve, J. Drewes, F. Schütt, R. Adelung, H. Kersten, *Plasma Processes Polym.* **2023**;20:e2200118.
<https://doi.org/10.1002/ppap.202200118>